The Meteoritical Society

Meteoritics & Planetary Science 57, Nr 2, 381–391 (2022)
doi: 10.1111/maps.13765

Fayalite formation through hydrothermal experiments: Insights into early fluid-assisted aqueous alteration processes on asteroids

E. DOBRICĂ [1*], J. A. NUTH[2], and A. J. BREARLEY [3]

[1]Hawai'i Institute of Geophysics and Planetology, School of Ocean, Earth Science, and Technology, University of Hawai'i at Mānoa, Honolulu, Hawaii 96822, USA
[2]Solar System Exploration Division, Code 690, NASA Goddard Space Flight Center, Greenbelt, Maryland 20771, USA
[3]Department of Earth and Planetary Sciences, MSC03-2040, 1 University of New Mexico, Albuquerque, New Mexico 87131–0001, USA
[*]Corresponding author. E-mail: dobrica@hawaii.edu

(Received 15 January 2021; revision accepted 27 October 2021)

Abstract–In order to understand the effects of the earliest fluid-assisted hydration processes on asteroids, we performed one hydrothermal experiment using three different reactants (FeO-rich amorphous silicates, iron metal powder, and water) at conditions informed by our current state of knowledge of asteroidal alteration. This experiment provides, for the first time, clear evidence that the growth of fayalite can occur during hydrothermal alteration, as described previously in meteorites. These newly formed fayalite crystals are elongated and porous, similar to the ones described in CV3, CK, and ordinary chondrites. The results show that (1) fayalite could form even if chemical equilibrium was not reached in the experiment, at a water to rock mass ratio (0.4 W/R at the beginning of the experiment) higher than the values calculated to be thermodynamically viable at equilibrium (W/R > 0.2); (2) the composition and the texture of the reactants changed during the hydrothermal alteration process, suggesting that the reactants, especially the amorphous silicates, underwent dissolution and reprecipitation; (3) fayalite can form at low temperature (220 °C), which is at the transition between hydrothermal alteration and fluid-assisted metamorphism in chondrites. The results are consistent with previous mineralogical observations and thermodynamic models, which suggest that fayalite crystals are formed on asteroidal parent bodies by the interaction between a hydrothermal fluid and disequilibrium assemblages that compose the pristine materials that condensed in the early solar nebula. This experiment suggests that two variables play a very important role in the formation of fayalite during the hydrothermal growth (W/R mass ratio and the fluid composition). These results are similar to the recent observations of the fine-grained matrix of ordinary chondrites.

INTRODUCTION

Iron-rich olivine (FeO-rich olivine: Fa_{50-100}, which spans a range from ferroan olivine ~Fa_{50} to pure fayalite Fa_{90-100}) is one of the major minerals in the matrices of unequilibrated ordinary (UOCs) and carbonaceous (CV, CK, CO) chondrites whose petrologic type is ≥3.05 (Abe et al., 2011; Brearley & Krot, 2013; Dobrică & Brearley, 2011, 2014, 2021; Doyle et al., 2015; Krot et al., 2004; Zolensky & Ivanov, 2003). Additionally, FeO-rich olivine has been detected in cometary materials (Frank et al., 2014; Joswiak et al., 2012; Lisse et al., 2006; Zolensky et al., 2008). Although there are several studies addressing the formation mechanism of FeO-rich olivine, its origin is still incompletely understood. Earlier studies argued that FeO-rich olivines were the products of gas–solid condensation in the solar nebula (Palme & Fegley, 1990; Weisberg et al., 1997; Weisberg & Prinz, 1998). However, more recent studies disputed this argument based on mineralogical observations, thermodynamic considerations, oxygen isotopic measurements, and the

fact that FeO-rich olivines are not present in very low petrologic type chondrites (<3.05; Brunner & Brearley, 2011; Dobrică & Brearley, 2011, 2020, 2021; Doyle et al., 2015; Fedkin & Grossman, 2006; Krot et al., 2004; Krot, Petaev, Scott, et al., 1998; Krot, Petaev, Zolensky, et al., 1998; Zolotov et al., 2006). A significant body of evidence exists that supports the view that FeO-rich olivines in chondrite matrices are the products of secondary asteroidal processes (Brunner & Brearley, 2011; Dobrică & Brearley, 2014, 2021; Doyle et al., 2015; Krot et al., 2004; Zolotov et al., 2006).

The formation of ferroan olivine during the aqueous alteration of chondrites has been demonstrated to be thermodynamically viable based on the calculations of Zolotov et al. (2006). The stability of ferroan olivine is highly dependent on several variables, including temperature, W/R mass ratio, pressure, hydrogen fugacity, and bulk rock composition. Additionally, hydrothermal growth during fluid-assisted metamorphism has been proposed as a mechanism for the formation of elongated FeO-rich olivine crystals in carbonaceous chondrite matrices (Abreu & Brearley, 2011; Brearley, 2009; Krot et al., 2004; Pontoppidan & Brearley, 2010). Dobrica and Brearley (2014) showed that amphibole and elongated FeO-rich olivines in the Tieschitz H3.6 chondrite formed contemporaneously, supporting the thermodynamic calculations of Zolotov et al. (2006) that ferroan olivines can form in the presence of fluids. Recently, Dobrica and Brearley (2021) showed, for the first time, the occurrence of FeO-rich olivines in a very low petrologic type chondrite (MET 00526, L3.05) as distinct submicron veins that crosscut regions of matrix consisting of amorphous silicates and phyllosilicates, providing evidence for aqueous fluid mass transport in a hydrothermal fluid.

In terrestrial rocks, fayalite is well known in plutonic and volcanic igneous rocks of high Fe:Mg ratios, such as ferrogabbro, ferrodiorite, syenite, and granite (Rasmussen et al., 1998). In metamorphic rocks, fayalite is a product of high-grade contact and regional metamorphism of banded iron formation and high-(Fe/Mg) igneous protoliths, where pressures were lower than those required to replace fayalite with ferrosilite (Rasmussen et al., 1998). However, at low to medium metamorphic grades, though at much higher pressures than those observed on the parent bodies of metamorphosed chondrites, fayalite is ordinarily not thermodynamically stable in FeO-rich metasediments for two reasons—the presence of quartz and an aqueous or carbonic pore fluid (Rasmussen et al., 1998). So far, hydrothermal alteration experiments have not been successful in forming FeO-rich olivines with the compositions and textures observed in the matrices of chondrites (Chizmadia et al., 2006; Le Guillou et al., 2015; Nakamura-Messenger et al., 2011). Therefore, unraveling the formation conditions of FeO-rich olivines remains a key problem to understand the effects of hydrothermal alteration on the high disequilibrium assemblages that compose the pristine chondrite matrices formed in the solar nebula (Brearley, 1993). We performed one hydrothermal experiment at optimal conditions of asteroidal parent bodies with the objective of synthesizing FeO-rich olivines to constrain their conditions of formation. In this study, we describe the results of this hydrothermal experiment and the implications for understanding the chemical reactions and the role of fluids in the fluid-assisted metamorphism that affected the matrices of ordinary and carbonaceous chondrites.

METHODS

The reactants (Fig. 1) and products (Figs. 2 and 3) of the hydrothermal experiment were examined by scanning electron microscopy (SEM) using an FEI Quanta 3D Dualbeam® focused ion beam (FIB) instrument operating at 30 kV. After detailed SEM characterization, electron transparent sections of five representative regions containing the new phases of the experimental run products were prepared using the in situ FIB technique (Fig. 3). A platinum protective layer (2 μm in thickness and 2 μm in width) was deposited on top of the regions of interest to avoid ion beam damage during the FIB sample preparation. The sections were transferred to copper FIB lift-out grids with an Omniprobe 200 micromanipulator. The final ion milling of the 2 μm thick section (~20 μm in length and ~6 μm in width) to electron transparency was carried out with the sample attached to the copper grid. The final thinning stages were performed at 5 kV with a Ga ion beam current of 10 pA. All FIB sections analyzed in this study are thicker (≳150 μm) than regular electron transparent materials since the samples are extremely porous and fragile. Due to the high porosity and the different degrees of ion sputtering between the mineral phases, some regions might be thinner than others. Each FIB section was studied using a variety of transmission electron microscopy (TEM) modes, including bright-field TEM imaging, high-angle annular dark-field scanning transmission electron microscopy (HAADF-STEM), selected area electron diffraction (SAED), and energy-dispersive X-ray spectroscopy (EDS). All imaging and analyses were carried out at 200 kV on a JEOL 2010F FEGTEM/Scanning TEM. In situ EDS X-ray analyses and maps were obtained using an Oxford Instruments AZtec EDS system equipped with an Oxford X-Max^N 80T 80 mm^2 EDS detector. The Cliff–Lorimer thin-film approximation was used for the

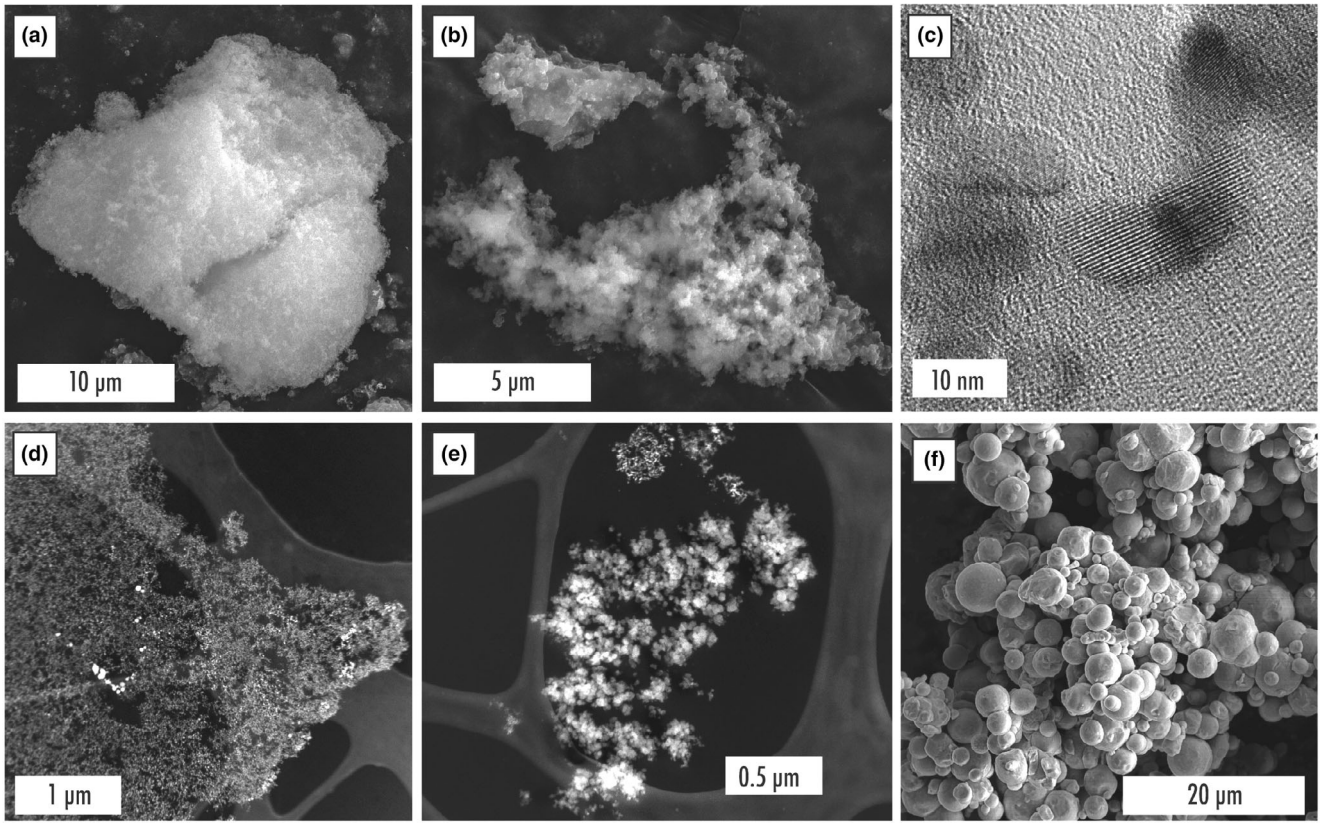

Fig. 1. Electron microscope images showing the texture of the reactants used in the experiment. a) Secondary electron images made by scanning electron microscopy (SEM) showing compact (a) and fluffy (b) iron-bearing, amorphous silicates. This condensed material has a variable chemical composition of FeO_y and SiO_x (avg. SiO_2 65 wt% and FeO 35 wt%, avg. atomic Fe/Si 0.5).c) High-resolution transmission electron microscope (TEM) image showing rare nanocrystalline regions identified in the amorphous silicates.d and e) Dark-field scanning transmission electron microscopy (DF-STEM) images of the compact (d) and fluffy (e) aggregates of amorphous silicates. f) Secondary electron image of the spherical iron metal powder (<10 μm) used as the source of iron for the hydrothermal experiment.

quantification of EDS data using theoretically determined k-factors. The individual EDS analyses were obtained by rastering the electron beam over the region or grain of interest (~10–100 nm) in STEM mode to minimize electron beam damage to the sample.

STARTING MATERIALS: REACTANTS

Three different reactants were used in this experiment —(1) FeO-rich amorphous silicates (Figs. 1a–e), (2) iron metal powder (Fig. 1f), and (3) water. No magnesium was present in the experiment. The FeO-rich amorphous silicates were synthesized experimentally by disequilibrium condensation from an Fe-SiO_2-H_2 vapor (Kimura & Nuth, 2007; Nuth et al., 2002). These amorphous silicates were produced at a total pressure of ~90 Torr in an atmosphere dominated by hydrogen (H_2 = 100, Si:O_2 = 20, Fe = 30) at temperatures between 425 and 450 °C (Nuth et al., 2002). Their compositions were measured by EDS/TEM (Table 1 and black circles from Fig. 4). These FeO-rich amorphous silicates have an intermediate chemical composition of FeO_y and SiO_x (avg. 65 wt% SiO_2 and 35 wt% FeO, avg. atomic Fe/Si 0.5, avg. pink circle Fig. 4b). They occur in compact and fluffy aggregates (Figs. 1a–e). Typical fluffy grains are on the order of 20–30 nm in diameter (Fig. 1e). Rare nanocrystalline regions were identified in the synthetic amorphous silicates (Fig. 1c). We chose this material as one of the reactants for the hydrothermal experiment since amorphous silicates are ubiquitous in almost all primitive solar system objects (chondritic meteorites and interplanetary dust particles) and in many astrophysical environments (Abreu & Brearley, 2010; Bockelée-Morvan et al., 2002; Bradley et al., 1999; Brearley, 1993; Chizmadia & Brearley, 2008; Dobrică & Brearley, 2012, 2020; Greshake, 1997; Keller & Messenger, 2011; Kemper et al., 2004; Le Guillou et al., 2014). Moreover, they are considered the major dust

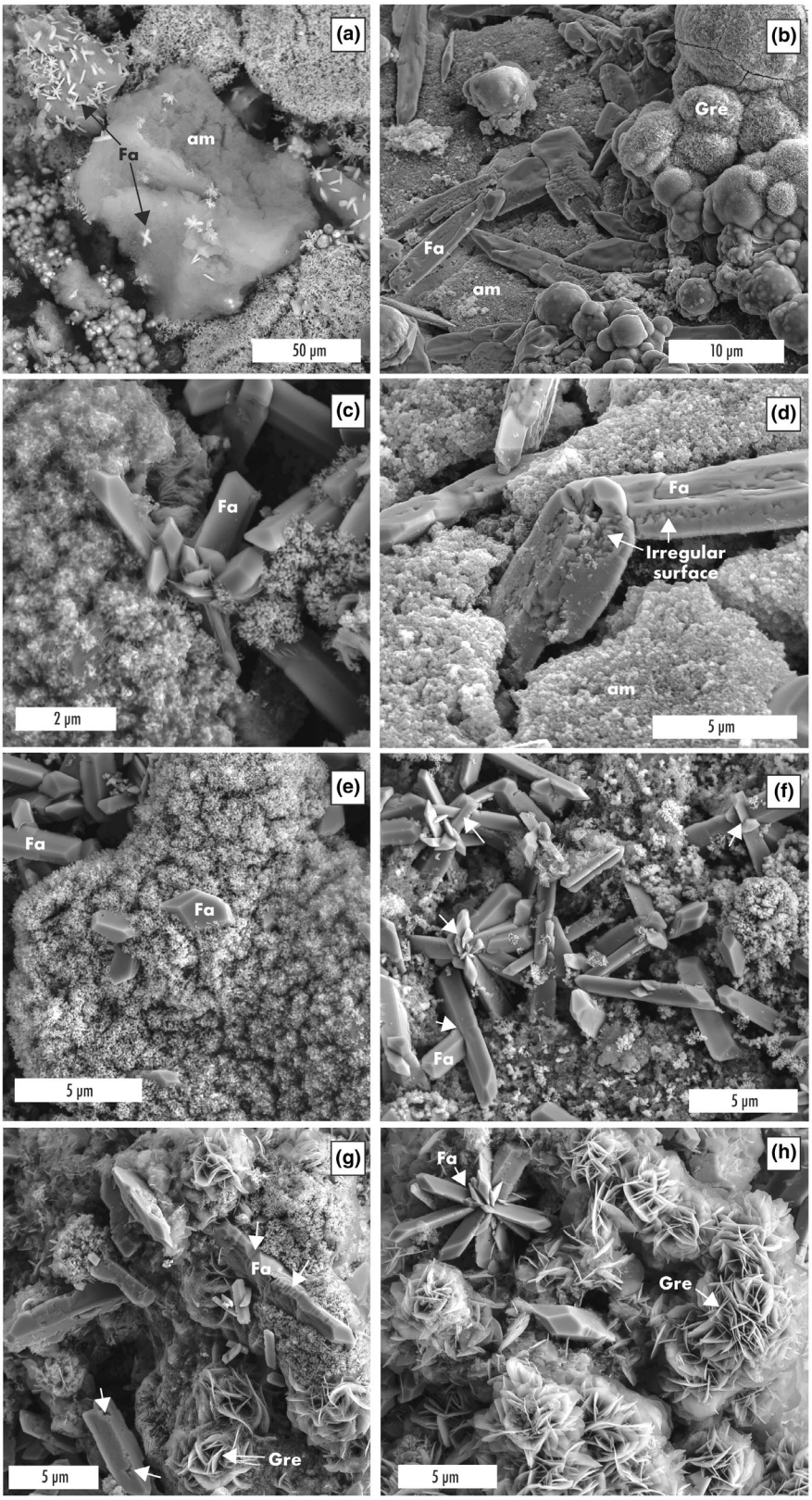
(a)
Fa
am
50 μm
(b)
Gre
Fa
am
10 μm
(c)
Fa
2 μm
(d)
Fa
Irregular surface
am
5 μm
(e)
Fa
Fa
5 μm
(f)
Fa
5 μm
(g)
Fa
Gre
5 μm
(h)
Fa
Gre
5 μm

Fig. 2. Backscattered (a, BSE) and secondary electron (b–h, SE) micrographs of the hydrothermal experiment products, fayalite (Fa), greenalite (Gre), and amorphous silicates (am). Part (b) shows the association of all these phases. The fayalite crystals are euhedral, elongated (b, d, and f–h), or prismatic (e) with sizes up to ~18 μm in length and ~2 μm wide. Their surfaces are either smooth (c, f) or irregular (d, g, white arrows). Radiating intergrowths of fayalite crystals (h—top, left and f—white arrows) are ubiquitous in the hydrothermal experiment. Greenalite was also identified in the products of the hydrothermal experiment (b, g–h). Their texture is a platy, radiating rose-like aggregate (g–h); however, rare fine-grained, platy crystals are present (b). The amorphous silicates are compact and homogeneous in texture (a, d). Generally, they are found associated with elongated fayalite crystals.

components of the solar system (Bockelée-Morvan et al., 2002; Bradley et al., 1999; Keller & Messenger, 2011; Van Boekel et al., 2004). They are found associated with FeO-rich olivine and hydrated phases in UOCs and are susceptible to aqueous alteration (Dobrica & Brearley, 2021). Additionally, their abundance decreases with the increase of the abundance of FeO-rich olivine in the matrices of type 3 chondrites as a function of the petrologic type (Dobrică et al., 2019; Pontippidan & Brearley, 2010). In CR2 chondrites, which are unmetamorphosed and are all petrologic type 2s, the abundance of amorphous silicates generally decreases as aqueous alteration becomes more advanced, due to the formation of phyllosilicates (Brearley & Krot, 2013; Brunner & Brearley, 2011; Le Guillou et al., 2015).

The second reactant used in this hydrothermal experiment is an iron metal powder (spherical particles, <10 μm, Fig. 1f). We added the iron metal powder to the experiments since (1) metallic Fe is one of the three most abundant components in chondrites that formed by condensation in the solar nebula (<0.1–70%; Scott & Krot, 2014), (2) is highly susceptible to aqueous alteration (Brearley, 2006), and (3) because the SiO_2/(SiO_2+FeO) ratios of the amorphous silicates used in this experiment are too silica-rich (avg. atomic Fe/Si and Mg/Si 0.5) to stabilize fayalite according to the T–$X(SiO_2)$ diagram (Fig. 4a) of Rasmussen et al. (1998). Therefore, in order to obtain a lower bulk SiO_2/(SiO_2+FeO) ratio, we added iron metal powder (spherical particles, <10 μm) to the system to reduce the bulk SiO_2/(FeO+SiO_2) ratio to <0.25 (the value at which fayalite becomes stable according to Rasmussen et al., 1998). The total Fe/Si ratio in the experiment was 7.8.

The last reactant used in the hydrothermal experiment is deionized water (18 MΩ) from which we removed dissolved oxygen using nitrogen (ultra-high purity grade) purging. Butler et al. (1994) show that nitrogen purging for 20–40 min at a flow rate of 25 mL s^{-1} is the most effective oxygen removal method. The concentration of residual dissolved oxygen after purging for ~30 min with nitrogen is 0.2–0.4 ppm (Butler et al., 1994). At the beginning of the hydrothermal experiment performed in this study, the W/R mass ratio was 0.4.

EXPERIMENTAL SETUP

We performed one hydrothermal experiment to synthesize FeO-rich olivines. We loaded the reactants (~3 mg of amorphous silicate, ~11 mg of iron metal powder, and 6 μL of water) in a gold (Au) capsule of ~230 mm^3 in volume. We sealed the gold capsule at room temperature and pressure in a glove box purged with N_2. The gold capsule was welded outside the glove box using a carbon pulse welder. The capsule was placed in a reactor vessel (Parr bomb) and heated in a low-temperature furnace (Fisher Scientific, Isotemp 500 Series). Deionized water was added inside the reactor vessel as a pressure medium (the water saturation pressure during the experiments was ~2300 kPa). The experiment was carried out at a temperature of 220 °C for 6 days. We tested whether the experiment was successful or not (e.g., leaks) by weighing the capsule before and after the experiment. Subsequently, the materials inside the gold capsule were deposited onto carbon tape and were studied by SEM before the more detailed FIB/TEM analysis.

RESULTS

Based on the SEM observations, multiple new phases were observed in the experimental products. Figure 2 shows the association of euhedral, FeO-rich crystals with homogeneous, low-Z material (Fig. 2a), and with platy, radiating rose-like aggregates (Figs. 2g and 2h). The FeO-rich crystals are observed either (1) as single, prismatic crystals embedded in the homogenous, low-Z material (Figs. 2a and 2e) or (2) as elongated, radiating intergrowths of multiple fayalite crystals (Figs. 2b, 2f, and 2h). The size of the prismatic crystals varies from a few hundreds of nanometers, up to ~2.7 × 1.5 μm. The elongated crystals have sizes up to ~18 μm in length and ~2 μm wide. The width of the elongated crystals (0.5–1.0 μm, SD 0.1) varies less than the length (0.8–18 μm, SD 1.3). Their surfaces are either smooth (Figs. 2c and 2f) or irregular (Figs. 2d and 2g, white arrows). Radiating intergrowths are ubiquitous in the hydrothermal experiment (Figs. 2f and 2h). The platy crystals in the radiating rose-like aggregates have

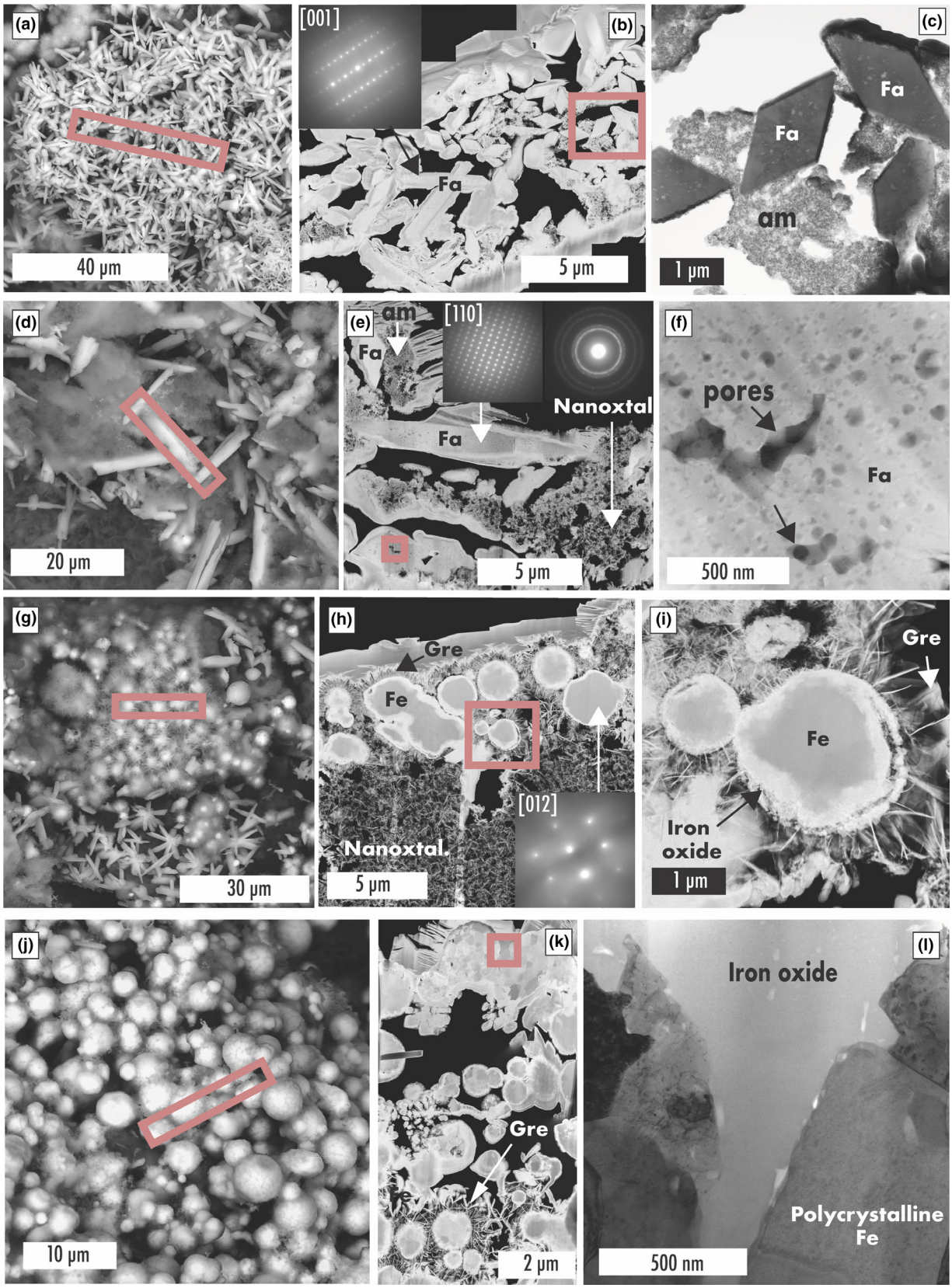
(a)
40 μm
[001]
(b)
Fa
5 μm
(c)
Fa
Fa
am
1 μm
(d)
20 μm
(e)
am
Fa
[110]
Nanoxtal
Fa
5 μm
(f)
pores
Fa
500 nm
(g)
30 μm
(h)
Gre
Fe
[012]
Nanoxtal.
5 μm
(i)
Gre
Fe
Iron
oxide
1 μm
(j)
10 μm
(k)
Gre
Fe
2 μm
(l)
Iron oxide
Polycrystalline
Fe
500 nm

Fig. 3. Backscattered electron (BSE, a, d, g, and j), dark-field (b, e, f, h, i, and k), and bright-field (c and l) micrographs made by scanning electron microscopy (SEM) and scanning transmission electron microscopy (STEM) showing the texture and the mineralogy of the hydrothermal experimental products. The pink rectangles show the regions where the focused ion beam (FIB) sections were prepared for TEM studies. The pink squares outline (b, e, h, and k) the areas shown in (c), (f), (i), and (l). Euhedral fayalite (Fa) crystals are observed in two FIB sections (b and e). Two diffraction patterns were indexed as [001] (b) and [110] (f) zone axis of fayalite (d). All fayalite crystals are porous (f) with length up to 750 nm. They are found associated with amorphous silicates (am. c) and nanocrystalline silicates (e—nanoxtal. diffraction rings). Additionally, we identified greenalite (Gre) crystals around the iron metal powder (g, h, see acicular crystals). The iron metal powder added as a reactant to the hydrothermal experiment was not completely consumed (g–i). However, the rims of the iron metal powder particles are transformed into iron oxide (i, l). Minerals identified in the FIB sections: Fa = fayalite; am = amorphous silicates; Fe = iron metal powder; Gre = greenalite. (Color figure can be viewed at wileyonlinelibrary.com.)

Table 1. Major and minor element compositions (wt% oxide, atom%, and structural formulae*) determined by energy-dispersive X-ray spectroscopy (EDS) of the amorphous silicate reactants (Am. react.) and products (Am. prod. = amorphous products; Nanoxtal. = nanocrystalline silicates; Gre. = Greenalite; Fa = Fayalite) identified in the focused ion beam (FIB) sections.

	Am. reac.		Am. prod.		Nanoxtal		Gre		Fa	
N	10	SD	9	SD	4	SD	4	SD	13	SD
SiO_2	64.5	2.4	40.2	6.4	44.6	1.6	35.2	1.0	30.3	0.6
FeO	35.5	2.4	59.8	6.4	55.4	1.6	64.8	1.0	69.7	0.6
Si	19.4	1.8	16.8	3.1	16.7	4.1	13.2	1.0	14.5	0.8
Fe	8.9	0.6	21.5	5.7	17.4	4.2	20.3	1.1	28.0	1.3
O	71.7	2.0	61.7	7.1	65.9	8.3	66.6	2.0	57.5	2.0
Si					2.6		2.0		1.0	
Fe					2.7		3.1		2.0	

*Mineral formulae were calculated on the basis of 4 oxygen (O) for fayalite (Fa) and 9 O for greenalite and the nanocrystalline material.

sizes up to 2.5 μm in length and a homogeneous thickness of ~30 nm in all the experimental products.

Using quantitative EDS/TEM analysis and electron diffraction, the elongated crystals were identified as fayalite (Fa_{100}, Figs. 2 and 3; Table 1). Some of the fayalite crystals are elongated parallel to the [001] direction (Fig. 3); however, only a few grains have been analyzed by electron diffraction. The average length of the fayalite crystals in the FIB section is ~2.1 μm and the width is 0.7 μm (N = 10). All fayalite crystals are porous with pore sizes up to ~750 nm in length (Fig. 3f).

Additionally, we identified a homogeneous amorphous silicate associated with the fayalite crystals in the experimental products (Figs. 2 and 3). The amorphous silicates have a compact texture and a wide compositional range (26.7–49.6 wt% SiO_2, 50.4–73.3 wt% FeO, Fig. 4). Their composition is more enriched in iron (avg. 40.2 wt % SiO_2, SD 6.4 and 59.8 wt% FeO, SD 6.4, avg. atomic Fe/Si 1, Fig. 4, am. product avg.—pink triangle, and Table 1) than the original amorphous silicates used as reactants (avg. 64.5 wt% SiO_2, SD 2.4 and 35.5 wt% FeO, SD 2.4, avg. atomic Fe/Si 0.5, Fig. 4, am. reactant avg.—pink circle). Nanocrystalline silicates (nanoxtal.) were also identified associated with the fayalite crystals (see Fig. 3e, ring diffraction pattern). This nanocrystalline material is enriched in iron (nanoxtal. avg.—55.4 FeO wt%, 44.6 SiO_2 wt%, Fig. 4, pink diamond) compared with the amorphous silicate products of the experiment (am. product avg.—40.2 wt% SiO_2, 59.8 wt% FeO, Fig. 4, pink triangle).

The platy, radiating rose-like aggregates were identified as greenalite ($[Fe^{2+}, Fe^{3+}]_{2-3}Si_2O_5OH_4$), which is an endmember of the serpentine group (Figs. 3 and 4; Table 1). These greenalite crystals were identified only around the iron metal powder used as reactant (see Figs. 3h–k). The iron metal powder was identified using EDS and electron diffraction analysis and was not completely consumed in the hydrothermal experiment (Fig. 3i). Figure 3h shows an electron diffraction pattern of the [012] zone axis of iron. The rims of the iron metal powder were oxidized and transformed into iron oxide (Fig. 3h). Additionally, an amorphous iron oxide with ~6 wt% SiO_2 was identified interconnecting multiple iron metal powder grains (Fig. 3l).

DISCUSSION

Previous studies of carbonaceous and ordinary chondrite matrices suggested that FeO-rich olivine could form during fluid-assisted metamorphism (Abreu & Brearley, 2011; Dobrică & Brearley, 2014, 2021; Doyle et al., 2015; Krot et al., 1997; Zolotov et al., 2006). However, so far, the growth of FeO-rich olivines from hydrothermal fluids has not been demonstrated experimentally, except for olivine-structured phase $LiFePO_4$ and related compounds (e.g., $LiFePO_4$, $LiMnPO_4$, $LiCoPO_4$, $LiNiPO_4$, and $LiMgPO_4$, Chen et al., 2008). Our hydrothermal experiment provides, for the first time, clear evidence that hydrothermal growth of elongated FeO-rich olivine can occur during thermal metamorphism in the presence of a fluid, as described previously in chondrites (e.g., Tieschitz, H/L 3.6,

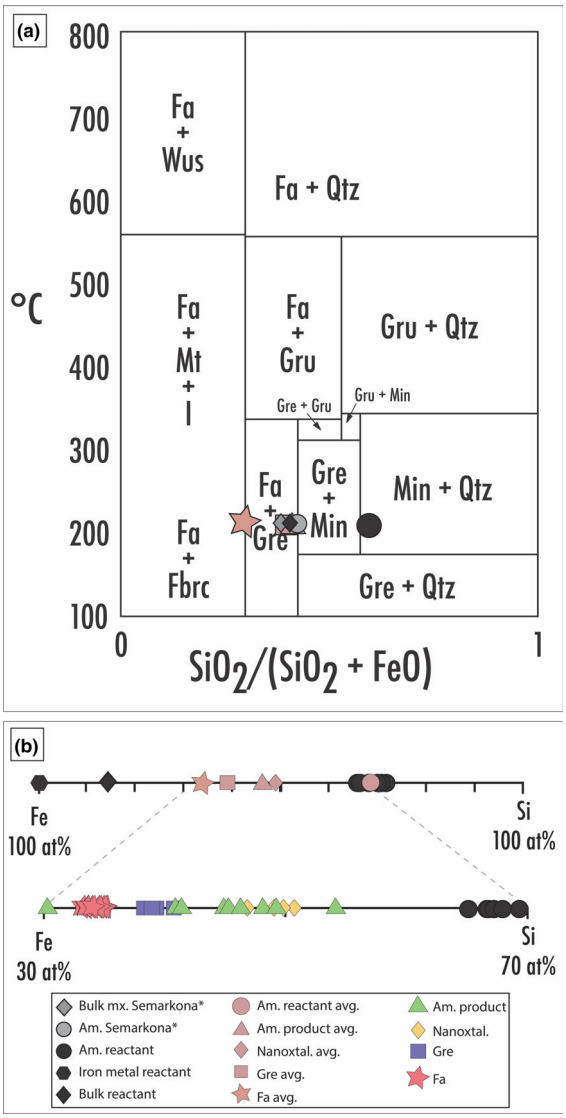

Fig. 4. a) Low-temperature, low-pressure phase relations in the system FeO-SiO_2-H_2O (FSH) from Rasmussen et al. (1998). SiO_2/(SiO_2+FeO) ratios versus temperature of the reactants. We plotted the average values of the amorphous silicate reactants (black circle), the bulk composition of the reactants (black diamond), and the products (average values greenalite—pink square; amorphous silicates—pink triangle; fayalite—pink star) of the hydrothermal experiment. For reference, we added the average chemical compositions of the bulk fine-grained matrix (gray diamonds) and the amorphous materials (gray circles) from Semarkona (Dobrică & Brearley, 2020).b) The atomic percentage of iron and silicon (atom%) of the reactants (amorphous silicate reactants—black circles, iron metal—black hexagons, bulk composition of the reactants—black diamonds) and products (greenalite—blue squares and avg. pink square; amorphous silicates—green triangles and avg. pink triangle; fayalite—red stars and avg. pink star; nanocrystalline—yellow diamonds and avg. pink diamond) of the hydrothermal experiment. Abbreviations: Am. = amorphous silicates; Fa = fayalite; Fbrc = iron analog of brucite; Gre = greenalite; Gru = grunerite; Min = minnesotaite; Mt = magnetite; Qtz = quartz; Wus = wüstite. (Color figure can be viewed at wileyonlinelibrary.com.)

Dobrică & Brearley, 2014). Additionally, these newly formed FeO-rich olivines have similar textures to the ones observed in chondrites. They are elongated, which is typical of CV3 matrix olivines (Allende and Kaba) and common in the FeO-rich olivines described in CK (NWA 1628) and OC (Tieschitz) meteorites (Brearley, 2009; Dobrică & Brearley, 2014; Krot et al., 1997; Watt et al., 2006; Weisberg et al., 1997). Furthermore, the FeO-rich olivines are porous similar to the ones described in CK and CV chondrites (Brearley, 1999, 2009). In CK chondrites, some of the pores contain ~100 nm grains of hydrous phases, which suggests that fluids may have played a role in the growth of olivines (Brearley, 2009). In addition to these characteristics that are familiar in other meteorites, the fayalite crystals formed during the hydrothermal experiment show frequent surface irregularities and multiple intergrowths. These morphologic characteristics of fayalite and their absence at the surface of FeO-rich olivine crystals identified in chondrites could indicate a change in the chemical composition of the fluid. Previous studies show that crystals growing in high supersaturation solutions have rougher, irregular surfaces (on a macroscopic rather than molecular scale) than those growing in low supersaturation solutions (Galbraith et al., 2016; Pantaraks et al., 2007). Although the difference in saturation for the chemical composition of the fluid in chondrites and the hydrothermal experiment cannot be disregarded, these morphologic characteristics could have been erased by subsequent metamorphic processes in chondrites (Allende, Kaba, and Tieschitz; Brearley, 2009; Dobrică & Brearley, 2014; Krot et al., 1997; Watt et al., 2006; Weisberg et al., 1997).

Additionally, the distribution and the chemical composition of fluid in the experiment may have been heterogeneous, and locally the W/R mass ratio was higher than the one intended in the experiment (0.4 W/R at the beginning of the experiment). This heterogeneity is suggested by the presence of regions in the sample (Fig. 3j) where the iron metal powder grains were not extensively modified during the experiments compared to regions where the abundance of secondary products (fayalite and greenalite) is much higher (Figs. 3a and 3d). This indicates that the W/R mass ratio controls the abundance of phases, though the temperature and the duration of the experiment have an important role in the type of phases formed during the experiment. Although the W/R mass ratio was not constrained during or after the experiment, we show that high W/R mass ratios are associated with regions where the abundance of secondary products is much higher. Additionally, since fayalite usually coexists with magnetite, except at a low W/R mass ratio (Zolotov et al., 2006), the lack of magnetite in this experiment could suggest that the W/R mass ratio in this experiment was high. However,

other factors could affect the formation of magnetite, such as the fluid composition (Fe/Si ratio), the redox conditions, and temperature (Zolotov et al., 2006). Therefore, we suggest that fayalite probably formed at a higher W/R mass ratio than the values measured at the beginning of the experiment (0.4 W/R). Furthermore, the presence of reactants associated with the products of the hydrothermal experiment demonstrates that the reactions took place under disequilibrium conditions. These observations are similar to our recent TEM study of the fine-grained matrix of MET 00526 (UOC, L3.05), showing the association of both reactants (amorphous silicates) and products (FeO-rich olivine and phyllosilicates) coexisting as high disequilibrium assemblages similar to the mineral assemblages in chondrite matrices (Brearley, 1993; Dobrică & Brearley, 2021). Previous studies have suggested that the distribution of water in some carbonaceous and ordinary chondrites was highly localized, rather than being pervasively distributed throughout the fine-grained matrix (Brearley, 2014; Dobrică et al., 2019; Le Guillou & Brearley, 2014). Therefore, our hydrothermal experiment shows similar local variations in the water content and fluid compositions as those described in chondrites. Note that the experiment performed in this study has been done in an ideal system, without magnesium, in contrast to the compositions of FeO-rich olivines in chondrites. Further experiments are in progress to understand the role of magnesium in the hydrothermal formation of FeO-rich olivines.

The fayalite crystals formed through the hydrothermal experiment are associated with amorphous silicates and phyllosilicates (greenalite), a mineral assemblage that is similar to what was recently described in unequilibrated ordinary chondrites (Dobrică & Brearley, 2021). Greenalite has rarely been described in chondrites, though it has been identified in CM chondrites (Barber, 1981; Rubin & Ma, 2017). The lack of magnesium in our hydrothermal experiment restrains the formation of phyllosilicates to the Fe-rich endmember of the serpentine group (greenalite) and not the Mg-serpentine that is ubiquitous in meteorites (Brearley & Krot, 2013; Dobrică & Brearley, 2021).

Multiple reaction mechanisms have been previously proposed to explain the asteroidal formation of FeO-rich olivine (Krot, Petaev, Scott, et al., 1998; Krot, Petaev, Zolensky, et al., 1998; Zolotov et al., 2006). However, three reaction mechanisms have been recently suggested by Dobrică and Brearley (2021) for the formation of FeO-rich olivine in UOCs, such as (1) replacement of amorphous silicates, (2) precipitation from an SiO_2-rich fluid, and (3) replacement of phyllosilicates. All these reaction mechanisms take place in the presence of an iron-, silica-rich fluid ($Fe^{2+}_{aqueous}$ and $SiO_{aqueous}$, see the schematic description and reaction mechanisms from Dobrică & Brearley, 2021). Although no direct measurements of the fluid composition were made during or after the hydrothermal experiment, the evolution of the fluid composition is confirmed by the changes observed in the composition and the texture of the original amorphous silicates used as reactants, which indicates that the primary amorphous material was partially dissolved in water and secondary silicate amorous material of different composition precipitated from solution. Figure 4 shows the variation in the chemical composition of the amorphous reactants (avg. pink triangle) and amorphous products (avg. pink circle) in the experiment, indicating an increase in the iron content during the hydrothermal reactions. This is similar to the results reported by Dobrică and Brearley (2021), which show that the chemical evolution of the hydrothermal fluid could trigger the formation of either fayalite or phyllosilicates depending on the Si/Fe ratios in the fluid (a.k.a. SiO2/[SiO2+FeO], Fig. 4). According to Rasmussen et al. (1998), a low Si/Fe ratio is required to form FeO-rich olivines, rather than phyllosilicates, which form at higher Si/Fe ratios. This relationship between the Si/Fe ratio and the formation of either olivine or phyllosilicates is represented in Fig. 4. Our hydrothermal experiment clearly shows mineral associations indicating that the fluid had locally variable compositions depending on the source of iron, to replace amorphous silicates at a low Si/Fe ratio and to form phyllosilicates at a high Si/Fe ratio. Additionally, our observations provide unequivocal evidence that fayalite forms in the presence of hydrothermal fluids with locally different chemical compositions (Si/Fe ratio) during the metamorphic evolution of the parent body of MET 00526.

CONCLUSION

Three significant outcomes occur from the hydrothermal experiment that was conducted at conditions that are informed by our current state of knowledge of asteroidal alteration. First, it shows that fayalite could form through disequilibrium reactions at W/R mass ratios higher than the values calculated to be thermodynamically viable at equilibrium (W/R mass ratio > 0.2, Zolotov et al., 2006). Second, the composition and the texture of the amorphous silicates used as reactants changed during the hydrothermal alteration process suggesting that the primary amorphous material was partially dissolved in water and secondary silicate amorous material of different composition precipitated during the experiment by an iron-rich fluid (Fe^{2+}). Third, fayalite can form at very low temperature (220 °C), which is at the transition between aqueous alteration and thermal metamorphism (Brearley & Krot, 2013). These three outcomes suggest that two variables appear to have a very important role in the formation of

fayalite during hydrothermal growth, namely, the W/R mass ratio and the fluid composition.

Acknowledgments—We thank the associate editor, Dr. M. Zolensky, and our reviewers, Dr. A. Rubin and Dr. M. Zolotov, for their insightful and constructive comments that helped to improve this manuscript. This work was funded by NASA grants NNH18ZDA001N-EW to E. Dobrica (PI) and NNX15AD28G to A. J. Brearley (PI). This is Hawaii Institute of Geophysics and Planetology publication No. HIGP 2451 and School of Ocean and Earth Science and Technology publication No. SOEST 11433.

Data Availability Statement—The data that support the findings of this study are available from the corresponding author upon reasonable request.

Editorial Handling—Dr. Michael Zolensky

REFERENCES

Abe, K., Sakamoto, N., Krot, A. N., and Yurimoto, H. 2011. Abundance of Cosmic Symplectite in Acfer 094 Carbonaceous Chondrite (abstract #9043). Formation of the First Solids in the Solar System Meeting.

Abreu, N. M., and Brearley, A. J. 2010. Early Solar System Processes Recorded in the Matrices of Two Highly Pristine CR3 Carbonaceous Chondrites, MET 00426 and QUE 99177. *Geochimica et Cosmochimica Acta* 74: 1146–71.

Abreu, N. M., and Brearley, A. J. 2011. Deciphering the Nebular and Asteroidal Record of Silicates and Organic Material in the Matrix of the Reduced CV3 Chondrite Vigarano. *Meteoritics & Planetary Science* 46: 252–74.

Barber, D. J. 1981. Matrix Phyllosilicates and Associated Minerals in C2M Carbonaceous Chondrites. *Geochimica et Cosmochimica Acta* 45: 945–70.

Bockelée-Morvan, D., Gautier, D., Hersant, F., Huré, J.-M., and Robert, F. 2002. Turbulent Radial Mixing in the Solar Nebula as the Source of Crystalline Silicates in Comets. *Astronomy & Astrophysics* 384: 1107–18.

Bradley, J. P., Keller, L. P., Snow, T. P., Hanner, M. S., Flynn, G. J., Gezo, J. C., Clemett, S. J., Brownlee, D. E., and Bowey, J. E. 1999. An Infrared Spectral Match Between GEMS and Interstellar Grains. *Science* 285: 1716–8.

Brearley, A. J. 1993. Matrix and Fine-Grained Rims in the Unequilibrated CO3 Chondrite, ALHA77307—Origins and Evidence for Diverse, Primitive Nebular Dust Components. *Geochimica et Cosmochimica Acta* 57: 1521–50.

Brearley, A. J. 1999. Origin of Graphitic Carbon and Pentlandite Inclusions in Matrix Olivines in the Allende Meteorite. *Science* 285: 1380–2.

Brearley, A. J. 2006. The Action of Water. In *Meteorites and the Early Solar System II*, edited by D. S. Lauretta and H. Y. McSween, 584–624. Tucson, Arizona: The University of Arizona Press.

Brearley, A. J. 2009. Matrix Olivines in the Metamorphosed CK Chondrite NWA 1628: Possible Affinities to Olivines in the Matrices of Oxidized CV3 Chondrites and Dark Inclusions (abstract #1791). 40th Lunar and Planetary Science Conference. CD-ROM.

Brearley, A. J., and Krot, A. N. 2013. Metasomatism in the Early Solar System: The Record from Chondritic Meteorites. In *Metasomatism and the Chemical Transformation of Rock*, edited by D. E. Harlov and H. Austrheim, 659–789. Berlin: Springer.

Brearley, A. J. 2014. Nebular versus parent body processing. In: Davis, A. M. (Ed.) *Meteorites and cosmochemical processes, treatise on geochemistry*, 2nd edition. Oxford: Elsevier-Pergamon, pp. 309–34.

Brunner, C. E., and Brearley, A. J. 2011. TEM Study of Matrix in the CO3 Chondrite ALHA 77307: Clues About the First Stages of Metamorphism in Chondrites. *Meteoritics & Planetary Science* 74(Suppl.): 5403.

Butler, I. B., Schoonen, M. A. A., and Rickard, D. T. 1994. Removal of Dissolved Oxygen from Water: A Comparison of Four Common Techniques. *Talanta* 41: 211–5.

Chen, J., Vacchio, M. J., Wang, S., Chernova, N., Zavalij, P. Y., and Whittingham, M. S. 2008. The Hydrothermal Synthesis and Characterization of Olivines and Related Compounds for Electrochemical Applications. *Solid State Ion* 178: 1676–93.

Chizmadia, L. J., and Brearley, A. J. 2008. Mineralogy, Aqueous Alteration, and Primitive Textural Characteristics of Fine-Grained Rims in the Y-791198 CM2 Carbonaceous Chondrite: TEM Observations and Comparison to ALHA81002. *Geochimica et Cosmochimica Acta* 72: 602–25.

Chizmadia, L. J., Nuth III, J. A., and Rietmeijer F. J. M. 2006. Experimental Aqueous Alteration of Amorphous Silicate Smokes (abstract #2187). 37th Lunar and Planetary Science Conference. CD-ROM.

Dobrică, E., and Brearley, A. J. 2011. Earliest Stages of Metamorphism and Aqueous Alteration Observed in the Fine-Grained Materials of Two Unequilibrated Ordinary Chondrites (abstract #2092). 42nd Lunar and Planetary Science Conference. CD-ROM.

Dobrică, E., and Brearley, A. J. 2012. Complex Heterogeneous Aqueous Alteration in the Matrices of Unequilibrated Ordinary Chondrites by Low Temperature Hydrothermal Solutions (abstract #2212). 43rd Lunar and Planetary Science Conference. CD-ROM.

Dobrică, E., and Brearley, A. J. 2014. Widespread Hydrothermal Alteration Minerals in the Fine-Grained Matrices of the Tieschitz Unequilibrated Ordinary Chondrite. *Meteoritics & Planetary Science* 49: 1323–49.

Dobrică, E., and Brearley, A. J. 2020. Amorphous Silicates in the Matrix of Semarkona: The First Evidence for the Localized Preservation of Pristine Matrix Materials in the Most Unequilibrated Ordinary Chondrites. *Meteoritics & Planetary Science* 54: 1973–89.

Dobrică, E., and Brearley, A. J. 2021. Iron-Rich Olivine in the Unequilibrated Ordinary Chondrite, MET 00526: Earliest Stages of Formation. *Meteoritics & Planetary Science* 55: 2652–69. https://doi.org/10.1111/maps.13610

Dobrică, E., Le Guillou, C., and Brearley, A. J. 2019. Aqueous Alteration of Porous Microchondrules in Semarkona: Implications for Hydration, Oxidation and Elemental Exchange Processes. *Geochimica et Cosmochimica Acta* 244: 292–307.

Doyle, P. M., Jogo, K., Nagashima, K., Krot, A. N., Wakita, S., Ciesla, F. J., and Hutcheon, I. D. 2015. Early Aqueous

Activity on the Ordinary and Carbonaceous Chondrite Parent Bodies Recorded by Fayalite. *Nature Communications* 6: 7444.

Fedkin, A. V., and Grossman, L. 2006. The Fayalite Content of Chondritic Olivine: Obstacle to Understanding the Condensation of Rocky Material. In *Meteorites and the Early Solar System II*, edited by D. S. Lauretta and H. Y. McSween Jr., 279–94. Tucson, Arizona: The University of Arizona Press.

Frank, D. R., Zolensky, M. E., and Le, L. 2014. Olivine in Terminal Particles of Stardust Aerogel Tracks and Analogous Grains in Chondrite Matrix. *Geochimica et Cosmochimica Acta* 142: 240–59.

Galbraith, S. C., Flood, A. E., Rugmai, S., and Chirawatkul, P. 2016. Relationship Between Surface Roughness, Internal Crystal Perfection, and Crystal Growth Rate. *Chemical Engineering and Technology* 39: 199–207.

Greshake, A. 1997. The Primitive Matrix Components of the Unique Carbonaceous Chondrite Acfer 094: A TEM Study. *Geochimica et Cosmochimica Acta* 61: 437–52.

Joswiak, D. J., Brownlee, D. E., Matrajt, G., Westphal, A. J., Snead, C. J., and Gainsforth, Z. 2012. Comprehensive Examination of Large Mineral and Rock Fragments in Stardust Tracks: Mineralogy, Analogous Extraterrestrial Materials, and Source Regions. *Meteoritics & Planetary Science* 47: 471–524.

Keller, L. P., and Messenger, S. 2011. On the Origins of GEMS Grains. *Geochimica et Cosmochimica Acta* 75: 5336–65.

Kemper, F., Vriend, W. J., and Tielens, A. G. G. M. 2004. The Absence of Crystalline Silicates in the Diffuse Interstellar Medium. *The Astrophysical Journal* 609: 826–37.

Kimura, Y., and Nuth, J. A. I. 2007. What Is the Driving Force to Form Refractory Oxide Grains? Silicate Spectra Depend on Their Formation Environment. *The Astrophysical Journal* 664: 1253–63.

Krot, A. N., Petaev, M. I., and Bland, P. A. 2004. Multiple Formation Mechanisms of Ferrous Olivine in CV Carbonaceous Chondrites During Fluid-Assisted Metamorphism. *Antarctic Meteorite Research* 17: 153.

Krot, A. N., Petaev, M. I., Scott, E. R. D., Choi, B.-G., Zolensky, M. E., and Keil, K. 1998. Progressive Alteration in CV3 Chondrites: More Evidence for Asteroidal Alteration. *Meteoritics & Planetary Science* 33: 1065–85.

Krot, A. N., Petaev, M. I., Zolensky, M. E., Keil, K., Scott, E. R. D., and Nakamura, K. 1998. Secondary Ca-Fe-Rich Minerals in the Bali-Like and Allende-Like Oxidized CV3 Chondrites and Allende Dark Inclusions. *Meteoritics & Planetary Science* 33: 623–45.

Krot, A. N., Scott, E. R. D., and Zolensky, M. E. 1997. Origin of Fayalitic Olivine Rims and Lath-Shaped Matrix Olivine in the CV3 Chondrite Allende and its Dark Inclusions. *Meteoritics & Planetary Science* 32: 31–49.

Le Guillou, C., Bernard, S., Brearley, A. J., and Remusat, L. 2014. Evolution of Organic Matter in Orgueil, Murchison and Renazzo During Parent Body Aqueous Alteration: In Situ Investigations. *Geochimica et Cosmochimica Acta* 131: 368–92.

Le Guillou, C., and Brearley, A. 2014. Relationships Between Organics, Water and Early Stages of Aqueous Alteration in the Pristine CR3.0 Chondrite MET 00426. *Geochimica et Cosmochimica Acta* 131: 344–67.

Le Guillou, C., Changela, H. G., and Brearley, A. J. 2015. Widespread Oxidized and Hydrated Amorphous Silicates in CR Chondrites Matrices: Implications for Alteration Conditions and H2 Degassing of Asteroids. *Earth and Planetary Science Letters* 420: 162–73.

Lisse, C. M., VanCleve, J., Adams, A. C., A'Hearn, M. F., Fernández, Y. R., Farnham, T. L., Armus, L. et al. 2006. Spitzer Spectral Observations of the Deep Impact Ejecta. *Science* 313: 635–40.

Nakamura-Messenger, K., Clemett, S. J., Messenger, S., and Keller, L. P. 2011. Experimental Aqueous Alteration of Cometary Dust. *Meteoritics & Planetary Science* 46: 843–56.

Nuth, J. A. I., Rietmeijer, F. J. M., and Hill, H. G. M. 2002. Condensation Processes in Astrophysical Environments: The Composition and Structure of Cometary Grains. *Meteoritics & Planetary Science* 37: 1579–90.

Palme, H., and Fegley Jr., B. 1990. High-Temperature Condensation of Iron-Rich Olivine in the Solar Nebula. *Earth and Planetary Science Letters* 101: 180–95.

Pantaraks, P., Matsuoka, M., and Flood, A. E. 2007. Effect of Growth Rate History on Current Crystal Growth. 2. Crystal Growth of Sucrose, $Al(SO_4)_2{\cdot}12H_2O$, KH_2PO_4, and K_2SO_4. *Crystal Growth & Design* 7: 2635–42.

Pontoppidan, K. M., and Brearley, A. J. 2010. Dust Particle Size Evolution. In *Protoplanetary Dust*, edited by D. Apai and D. Lauretta, 191–229. Cambridge, UK: Cambridge University Press.

Rasmussen, M. G., Evans, B. W., and Kuehner, S. M. 1998. Low-Temperature Fayalite, Greenalite, and Minnesotaite from the Overlook Gold Deposit, Washington; Phase Relations in the System $FeO\text{-}SiO_2\text{-}H_2O$. *Canadian Mineralogist* 36: 147–62.

Rubin, A. E., and Ma, C. 2017. Meteoritic Minerals and Their Origins. *Chemie der Erde—Geochemistry* 77: 325–85.

Scott, E. R. D., and Krot, A. N. 2014. Chondrites and Their Components. In *Meteorites and Cosmochemical Processes*, edited by A. M. Davis, 65–137. Treatise on Geochemistry, vol. 1. Oxford: Elsevier-Pergamon.

Van Boekel, R., Min, M., Leinert, C., Waters, L. B. F. M., Richichi, A., Chesneau, O., Dominik, C. et al. 2004. The Building Blocks of Planets Within the 'Terrestrial' Region of Protoplanetary Disks. *Nature* 432: 479–82.

Watt, L. E., Bland, P. A., Prior, D. J., and Russell, S. S. 2006. Fabric Analysis of Allende Matrix Using EBSD. *Meteoritics & Planetary Science* 41: 989–1001.

Weisberg, M. K., and Prinz, M. 1998. Fayalitic Olivine in CV3 Chondrite Matrix and Dark Inclusions: A Nebular Origin. *Meteoritics & Planetary Science* 33: 1087–99.

Weisberg, M. K., Zolensky, M. E., and Prinz, M. 1997. Fayalitic Olivine in Matrix of the Krymka LL3.1 Chondrite: Vapor-Solid Growth in the Solar Nebula. *Meteoritics & Planetary Science* 32: 791–801.

Zolensky, M., and Ivanov, A. 2003. The Kaidun Microbreccia Meteorite: A Harvest from the Inner and Outer Asteroid Belt. *Chemie der Erde* 63: 185–246.

Zolensky, M., Nakamura-Messenger, K., Rietmeijer, F., Leroux, H., Mikouchi, T., Ohsumi, K., Simon, S. et al. 2008. Comparing Wild 2 Particles to Chondrites and IDPs. *Meteoritics & Planetary Science* 43: 261–72.

Zolotov, M. Y., Mironenko, M. V., and Shock, E. L. 2006. Thermodynamic Constraints on Fayalite Formation on Parent Bodies of Chondrites. *Meteoritics & Planetary Science* 41: 1775–96.